Supplementary Material

Proof for the mathematical derivations for DDMPs with B-Maps

For DDPMs with B-Maps implementation, like the standard DDMP, the optimization is based on maximizing the Evidence Lower Bound (ELBO)[13]:

$$
\begin{aligned}
\log p(x) \geq & \mathbb{E}_{q(x_1|x_0)}[\log p_\theta(x_0|x_1)] - D_{KL}(q(x_T|x_0) \| p(x_T)) \\
& - \sum_{t=2}^{T} \mathbb{E}_{q(x_t|x_0)}[D_{KL}(q(x_{t-1}|x_t, x_0) \| p_\theta(x_{t-1}|x_t))]
\end{aligned} \tag{6}
$$

In this derivation of the ELBO, the bulk of the optimization cost lies in the summation term. By Bayes rule, we have: $q(x_{t-1}|x_t, x_0) = \frac{q(x_t|x_{t-1}, x_0) q(x_{t-1}|x_0)}{q(x_t|x_0)}$

where the first term in the nominator is known Eq. (2) and tractable. Recalling the reparameterization trick, the form of $q(x_t|x_0)$ and $q(x_{t-1}|x_0)$ can be recursively derived through repeated applications of the reparametrization trick.

$$
\begin{aligned}
& x_t = \sqrt{\alpha_t B_t} x_{t-1} + \sqrt{1 - \alpha_t B_t} \epsilon_{t-1}, \quad \text{where } \epsilon_{t-1} \sim \mathcal{N}(0, \mathbf{I}) \\
& = \sqrt{\alpha_t B_t} \sqrt{\alpha_{t-1} B_{t-1}} x_{t-2} + \underbrace{\sqrt{\alpha_t B_t} \sqrt{1 - (\alpha_{t-1} B_{t-1})} \epsilon_{t-2} + \sqrt{1 - (\alpha_t B_t)} \epsilon_{t-1}}_{(1)} \\
& = \sqrt{\alpha_t \alpha_{t-1} B_t B_{t-1}} x_{t-2} + \sqrt{1 - (\alpha_t \alpha_{t-1} B_t B_{t-1})} \epsilon_{t-2} \\
& = \ldots \\
& = \sqrt{\prod_{i=1}^{t} \alpha_i B_i} x_0 + \sqrt{1 - \prod_{i=1}^{t} \alpha_i B_i} \epsilon, \\
& \sim \mathcal{N}(x_t; \sqrt{\bar{\alpha}_t \bar{B}_t} x_0, (\mathbf{1} - \bar{\alpha}_t \bar{B}_t)
\end{aligned} \tag{7}
$$

Where, all multiplications are point-wise and in (1) we apply the fact that the sum of two independent Gaussian random variables remains a Gaussian with mean being the sum of the two means, and variance being the sum of the two variances. We have therefore derived like this the Gaussian form of $q(x_t|x_0)$, and we can derive $q(x_{t-1}|x_0)$ the same way. Therefore, knowing the forms of both $q(x_t|x_0)$ and $q(x_{t_1}|x_0)$, we can proceed to calculate the form of $q(x_{t_1}|x_t, x_0)$:

$$
\begin{aligned}
& q(x_{t-1}|x_t, x_0) = \frac{q(x_t|x_{t-1}, x_0) q(x_{t-1}|x_0)}{q(x_t|x_0)} \\
& = \frac{\mathcal{N}(x_t; \sqrt{\alpha_t B_t} x_{t-1}, (\mathbf{1} - \alpha_t B_t)\mathbf{I}) \mathcal{N}(x_{t-1}; \sqrt{\bar{\alpha}_{t-1} \bar{B}_{t-1}} x_0, (\mathbf{1} - \bar{\alpha}_{t-1} \bar{B}_{t-1})\mathbf{I})}{\mathcal{N}(x_t; \sqrt{\bar{\alpha}_t \bar{B}_t} x_0, (\mathbf{1} - \bar{\alpha}_t \bar{B}_t)\mathbf{I})}
\end{aligned} \tag{8}
$$

Following the same derivation as in [13] but with our modified Gaussian distributions that depend also on B, we arrive to the posterior distribution described in the paper.

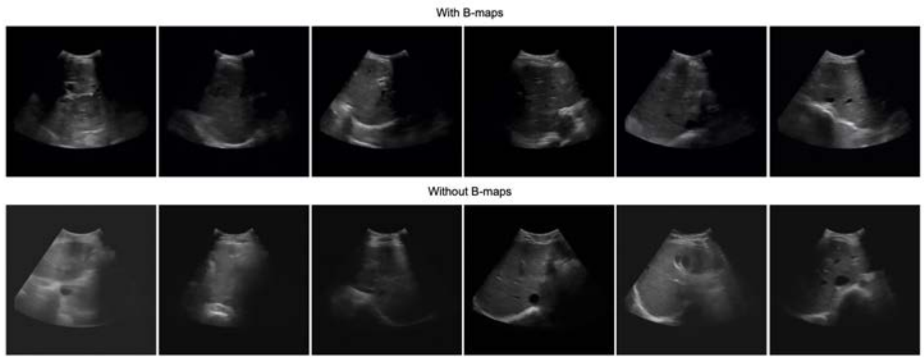

Fig. 5. Liver Results: US images generated with B-Maps (top) exhibit enhanced contrast, especially in the upper regions, compared to those without (bottom).

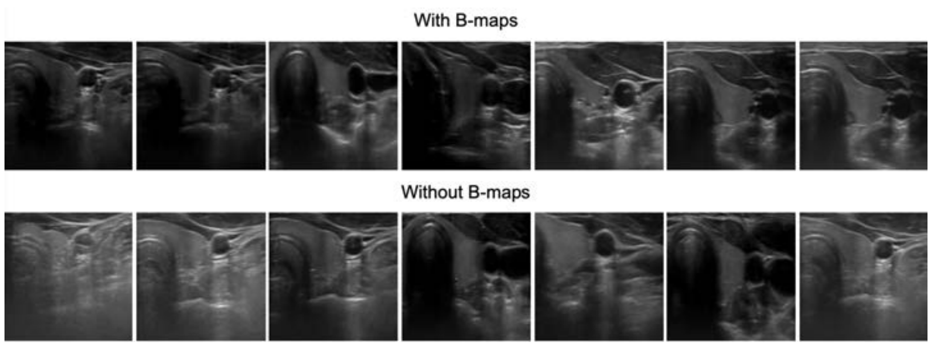

Fig. 6. Thyroid Results: The application of B-Maps in the generation of thyroid US images (top row) results in a clearer delineation and contrast, which is less pronounced in images generated without B-Maps (bottom row).

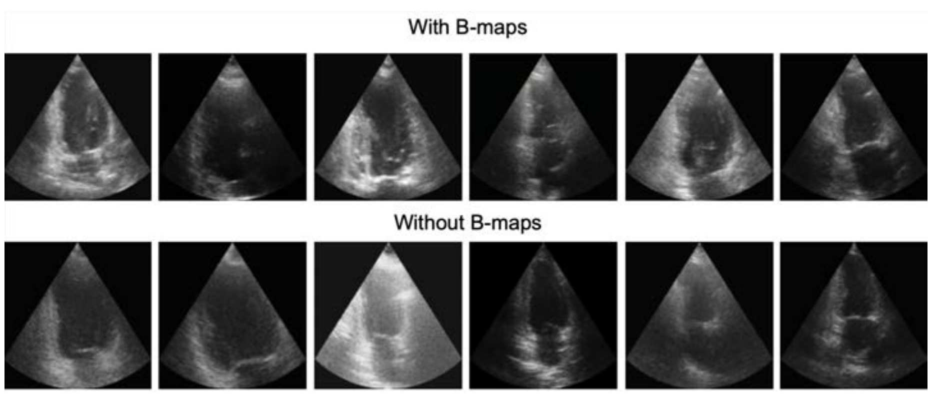

Fig. 7. CAMUS Results: Images generated with B-Maps (top row) have improved contrast in the superior sections, contrasting with the lower contrast seen in the images without B-Maps (bottom row).